Charge tunneling injection through a thin teflon film between the electrodes and organic semiconductor layer: Relation to...

Article *in* Physical Review B · October 2006

DOI: 10.1103/PhysRevB.74.165307

CITATIONS
14

READS
13

5 authors, including:

Zhaoxin Wu
Xi'an Jiaotong University
115 PUBLICATIONS **991** CITATIONS
SEE PROFILE

Liduo Wang
Tsinghua University
251 PUBLICATIONS **5,448** CITATIONS
SEE PROFILE

Charge tunneling injection through a thin teflon film between the electrodes and organic semiconductor layer: Relation to morphology of the teflon film

Zhaoxin Wu,[1,2] Liduo Wang,[2,*] Haifeng Wang,[2] Yudi Gao,[2] and Yong Qiu[2,†]
[1]*School of Electronic and Information Engineering, Xi'an Jiaotong University, Xi'an 710049, China*
[2]*Key Lab of Organic Optoelectronics & Molecular Engineering, Department of Chemistry, Tsinghua University, Beijing 100084, China*
(Received 25 October 2005; revised manuscript received 5 June 2006; published 6 October 2006)

The different behaviors of enhancement of charge injection of an organic electronic device were observed by the incorporation, into the device, of the flat and rough insulating layers (polytetrafluoroethylene) separating the indium tin oxide and organic semiconductor [tris(8-hydroxyquinoline) aluminum]. The observed charge injection enhancements can be explained by the carrier tunneling injection only when the morphology of the insulating layers was taken into account in the calculation based on the tunneling model. Our research in theory and experiment provided a further understanding of the carrier tunneling injection through the thin insulating film in organic electronic devices.

DOI: 10.1103/PhysRevB.74.165307 PACS number(s): 73.40.Ns, 72.80.Le, 73.40.Qv, 73.40.Gk

I. INTRODUCTION

The charge injection often plays a dominant role in electronic devices based on amorphous organic materials such as organic light-emitting diodes (OLEDs), thin film transistors, photodetectors, and solar cells. The efficiency of OLEDs is directly related to the ability of the contacts to supply the organic bulk with charge injection. It is generally recognized that the enhancement of carrier injection is essential for the high performance of devices. Much research has been conducted and it was found that carrier injection was enhanced by the insertion of a thin insulator with the optimal thickness between the electrode and the organic layer, such as poly(methylmethacrylate) (PMMA) LB films,[1] LiF,[2–6] CsF,[7] Al_2O_3,[8,9] NaCl,[10] sodium stearate (NaSt),[11] Si_3N_4,[12] and teflon[13] layers. There are different mechanisms for these phenomena. When LiF or CsF was used as the insulating layer and Al or Mg as the metallic cathode, dissociation of the LiF and CsF and subsequent "doping" of Li or Cs into the organic bulk were presented as a possible mechanism resulting in enhanced electron injection.[2,4,7,14] Besides, the charge tunneling effect was also considered to be an alternative underlying mechanism for the insulators such as PMMA,[1] LiF layer combined with Ag or ITO electrode,[3,5,6] Al_2O_3,[8] NaSt,[11] Si_3N_4,[12] and teflon.[13]

The model of charge tunneling through the barrier into organic semiconductor was presented by Parker *et al.*,[15] and based on this model, Kim *et al.*[1] then qualitatively proposed the principle of carrier tunneling through a thin insulating layer between the electrode and organic semiconductor layer. Recently, the corresponding theoretical model and calculations through the thin insulating layer were presented in Zhang *et al.*[16] Zhang's model successfully explained the enhancement of carrier injection using LiF layer combined with Ag and ITO electrodes,[3,5] and NaSt layer with Mg, Al, and Ag cathodes respectively.[17] However, Zhang's model was limited to the explanation of some experimental results; for example, the optimal thickness of the insulating layer for maximum carrier injection in the experiment was almost one order of magnitude larger than the theoretical results.[5] A reasonable understanding of carrier injection enhancement through insulation is therefore needed.

In this article, hole injection from indium-tin oxide (ITO) to tris(8-hydroxyquinoline) aluminum (Alq) through thin teflon films with different surface morphology was investigated experimentally and theoretically. The teflon films with different surface morphology were fabricated by means of sputtering and vacuum thermal evaporation. We found that hole injection was enhanced by the insertion of the teflon films. The injection current through the teflon film by the thermal evaporation in the device reached a maximum twice with different thicknesses of teflon film, which was quite different from the case by the sputtering as well as the cases of reported thin insulating films in previous literature.[5,6,12,17] In theory, we further developed Kim's and Zhang's models and found that our theoretical results, taking the morphology of teflon film into account, agreed well with the experimental ones. Our research showed that the morphology of teflon films is a critical factor for the enhancement of hole injection in OLEDs, leading to a further understanding of the physical process of carrier injection in OLEDs.

The article is organized as follows: in Sec. II we present the experimental results of hole injection enhancement from ITO to Alq through teflon films with different surface morphologies. In Sec. III, we describe the theoretical model for the calculation of tunneling current in the device, and the numerical simulation and explanation of experiments are given in Sec. IV. In the Appendix, the detailed steps to obtain theoretical model and numerical results are presented.

II. EXPERIMENTAL

In order to study the hole injection process from an ITO anode to an organic material (Alq) through a teflon film, a single-carrier-type, "hole-only" device was fabricated, where the current density of electrons was reduced to negligible levels by lowering the efficiency of the electron injecting contact. The hole-only device in our experiment was built on glass substrates precoated with ITO film and had a configuration of ITO/teflon (x nm)/Alq (60 nm)/N, N′-diphenyl-N,

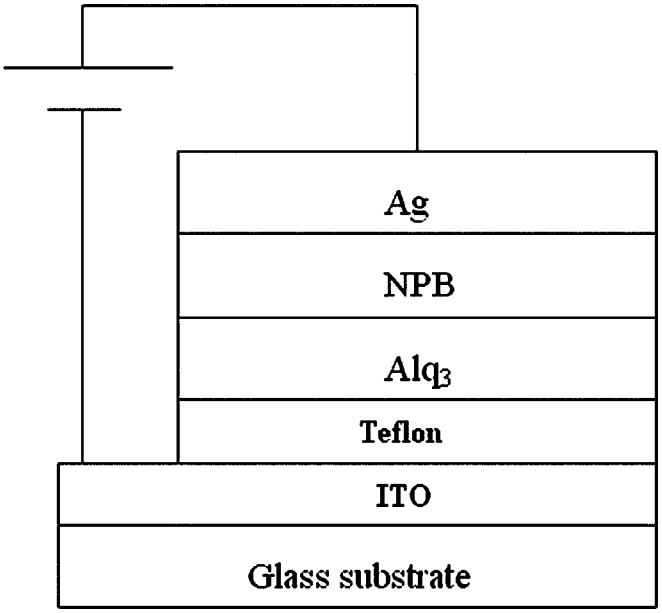

FIG. 1. Configuration of the hole-only device with ITO/Alq (60 nm)/NPB (20 nm)/Ag (200 nm).

N′-bis (1,1′-biphenyl)-4,4′-diamine (NPB) (20 nm)/Ag (200 nm), which is shown in Fig. 1. Silver was chosen as the cathode with Fermi energy of 4.6 eV, and NPB was used as an electron blocking layer with a lowest unoccupied molecular orbital (LUMO) level of 1.8 eV. The great offset between the Fermi energy of the cathode and the LUMO level of NPB served to reduce the efficiency of the electron injection and guarantee the holes injected from the anode would dominate in the device. The detailed fabrication of the devices was shown elsewhere.[13,18]

The morphologies of the teflon films fabricated by the sputtering are shown by atomic force microscope (AFM) in Fig. 2. Figure 2(a) shows the surface of ITO film on the glass substrate, and Figs. 2(b)–2(d) show the AFM images of the

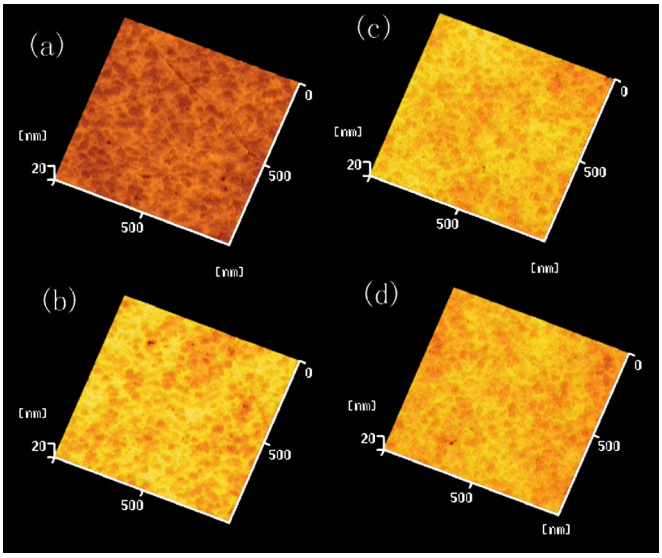

FIG. 2. (Color online) AFM images of (a) ITO film, (b) 0.5 nm thick, (c) 1 nm thick, and (d) 6 nm thick teflon films by sputtering.

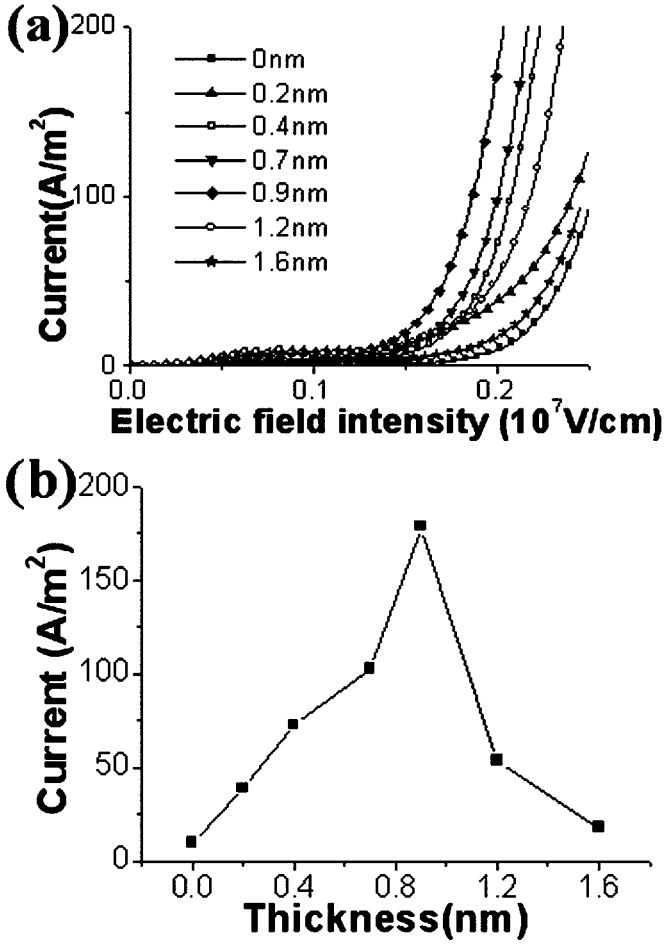

FIG. 3. (a) Thickness dependence of the *I-V* characteristics for the hole-only device with teflon films by sputtering. (b) The current of the hole-only device vs different thicknesses of teflon film (under electric field of 0.2×10^7 V/cm).

teflon film with thickness of 0.5 nm, 1 nm, and 6 nm. The root mean square (RMS) of the roughness of films in Figs. 2(a)–2(d) were 0.28 nm, 0.24 nm, 0.29 nm, and 0.27 nm, which show that teflon films by sputtering are quite smooth as ITO film. Figure 3(a) shows the current density versus voltages (*I-V*) characteristics of hole-only devices with different thicknesses of teflon film by sputtering, which were measured by the Keithley 4200. We observed that the injection current density was enhanced and reached maximum current density at the thickness of teflon film of 0.9 nm under an electric field of 0.2×10^7 V/cm, shown in Fig. 3(b).

Figure 4 shows the morphology of the teflon films fabricated by thermal evaporation. The surface of the teflon films by thermal evaporation was not a perfectly flat surface, but was somewhat rough. Figure 4(a) shows the surface of the ITO substrate, which was quite smooth. Figure 4(b) shows a 2 nm thick teflon layer. The teflon film measured as 2 nm did not fully cover the ITO substrate and islands of teflon on the ITO substrate were observed. Figure 4(c) shows a 4 nm thick teflon layer. Islands of teflon grew but did not form a continuous film. As for the 15 nm thick teflon layer in Fig. 4(d), coalescence of teflon islands occurred, forming a continuous teflon film on the ITO substrate. The RMS of the roughness

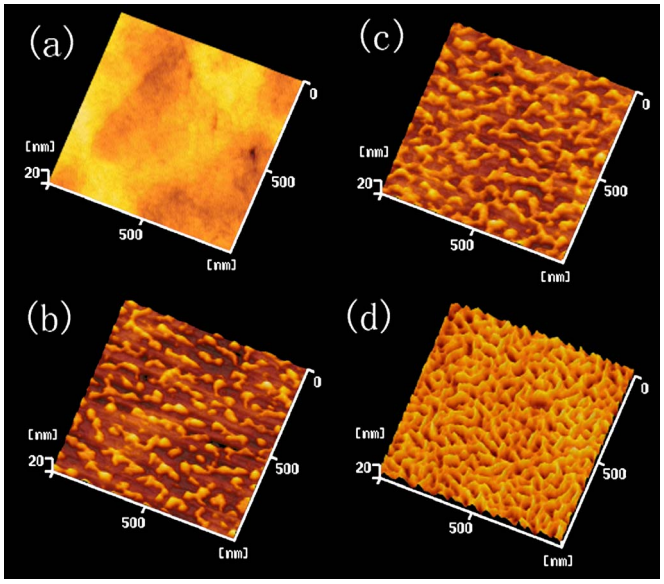

FIG. 4. (Color online) AFM images of (a) ITO film, (b) 2 nm thick, (c) 4 nm thick, and (d) 15 nm thick teflon films by vacuum thermal evaporation.

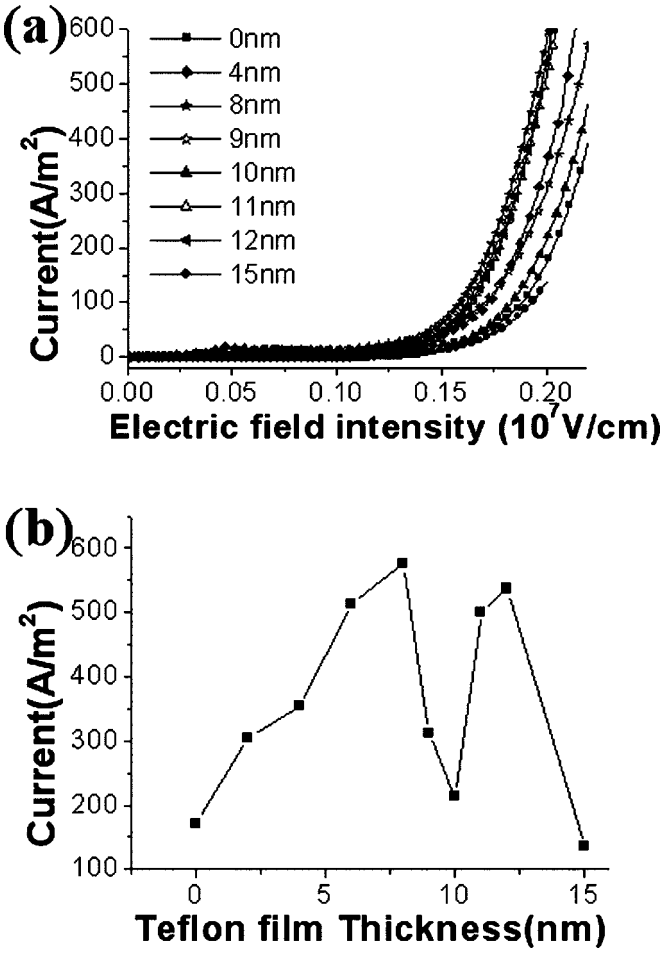

FIG. 5. (a) Thickness dependence of the *I-V* characteristics for the hole-only device with teflon films by thermal evaporation. (b) The current of the hole-only device vs different thicknesses of teflon film (under electric field of 0.2×10^7 V/cm).

of films in Figs. 4(a)–4(d) were 0.28 nm, 1.15 nm, 1.10 nm, and 2.7 nm.

Figure 5(a) shows *I-V* characteristics of hole-only devices with teflon films by thermal evaporation. It was observed that the current density was increased by the insertion of 2 nm, 4 nm, 6 nm, and 8 nm thick teflon film between Alq and ITO, and the maximum current densities were achieved when 8 nm and 12 nm thick teflon films were used. Figure 5(b) shows the current densities of devices with different thicknesses of teflon film under an electric field of 0.2×10^7 V/cm. The current density of the devices reached the maximum twice with 8 nm and 12 nm thick teflon film.

III. THEORETICAL MODEL

In order to analyze and understand the mechanism of the enhancement of hole injection from ITO to Alq through a thin teflon film, we started with a physical model based on the tunneling effect.[1,16] Figure 6 shows the energy diagram of our devices with and without a thin teflon film. The Fermi level of ITO was 4.7 eV, the highest occupied molecular orbital (HOMO) of Alq was 5.7 eV, and the HOMO of teflon film was measured as 9.8 eV.[13] In Fig. 6(a), if no thin teflon film was included, then upon application of a forward voltage, holes had to tunnel through a triangular energy barrier. In the presence of a thin teflon film with the proper thickness, the voltage drop across the teflon film decreased the difference between the Fermi level of ITO and HOMO of Alq and reduced the thickness of the energy barrier through which holes tunneled from ITO to Alq, thus increasing the injection current of holes. Based on the WKB approximation[19] and neglecting the interfacial state, the space charge limitation in Alq, we calculated the tunneling current from ITO to Alq through the teflon film in Fig. 6(b). In order to compare this with the experimental results in Figs. 3 and 5, we also calculated the average current density of holes from ITO to Alq through the surface S in devices in Fig. 7. The detailed theoretical model and calculation can be found in the Appendix of this article. The average current density $\bar{J}$ is shown as follows:

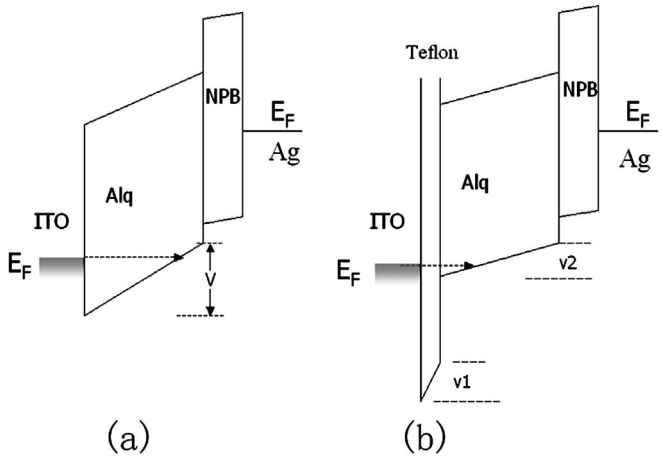

FIG. 6. Schematic of energy diagram of the device without (a) and with (b) thin teflon film.

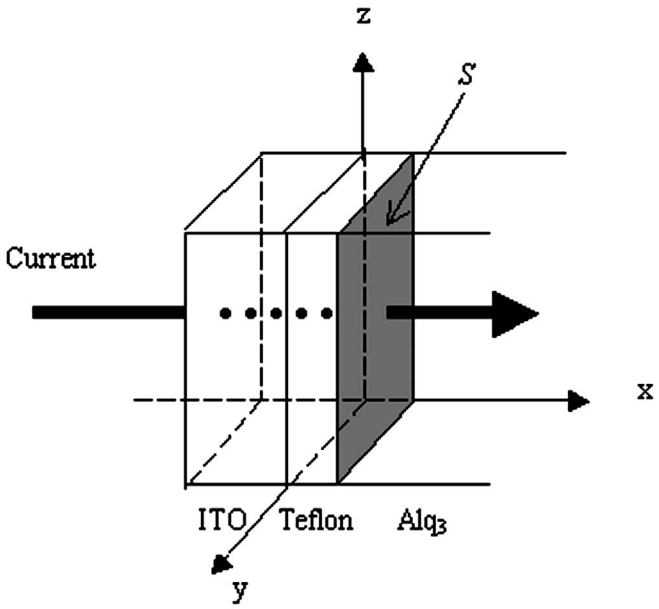

FIG. 7. Schematic of hole-tunneling injection from ITO into Alq through the surface S between teflon and Alq films.

$$\bar{J} = \left(\frac{K_b T}{2\pi^2 \hbar^3}\right)\left\{\iint \vec{e}_x \cdot \vec{n} ds dp_x p_x T(y,z,p_x) \times \ln\left[1 + \exp\left(\frac{E_f - p_x^2/2m}{K_b T}\right)\right]\right\}/S, \quad (1)$$

$$T(y,z,p_x) \approx \exp\left(-2\int_{x1}^{x2} \eta dx\right), \quad (2)$$

$$\eta = \left\{\frac{2m}{\hbar^2}\left[U(x,y,z) - \frac{p_x^2}{2m}\right]\right\}^{1/2}, \quad (3)$$

where p_x is the x component of the carrier momentum, $T(y,z,p_x)$ is the transmission coefficient at the position (y,z) on the surface S, $U(x,y,z)$ is the potential energy, E_f is the Fermi level of the ITO, m is the carrier effective mass, K_b is the Boltzmann constant, and $\hbar = h/2\pi$ is the Plank's constant. $\vec{n}$ is a unit vector normal to the area element ds of the surface S, and $\vec{e}_x$ is the unit vector of x direction

IV. NUMERICAL RESULTS AND DISCUSSION

In our calculation, the ratio of the resistances of teflon and Alq film was approximated to 3:1, which decided the ratio of drop voltages of teflon and Alq films by Ohmic law,[16] and then according to the energy diagram of ITO/teflon/Alq in Fig. 6, the potential energy $U(x,y,z)$ was determined for the given thickness of teflon layer, local electric field, and the positions of (y,z).

First, we considered the tunneling current through a perfectly flat teflon film in a hole-only device. If the teflon film was uniform and the surface S between teflon and Alq was perfectly flat, then the potential energy $U(x,y,z) = U(x)$, the transmission coefficient $T(y,z,p_x) = T(p_x)$, and tunneling current density $J(y,z) = J$ at the position (y,z) on the surface S were independent on the y and z component in space. Thus the average transmitting current density through the surface S is

$$\bar{J} = J = \left(\frac{K_b T}{2\pi^2 \hbar^3}\right)\int dp_x p_x T(p_x) \ln\left[1 + \exp\left(\frac{E_f - p_x^2/2m}{K_b T}\right)\right]. \quad (4)$$

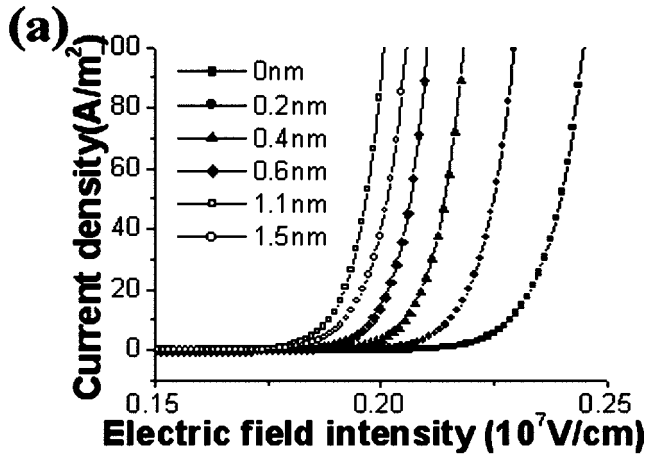

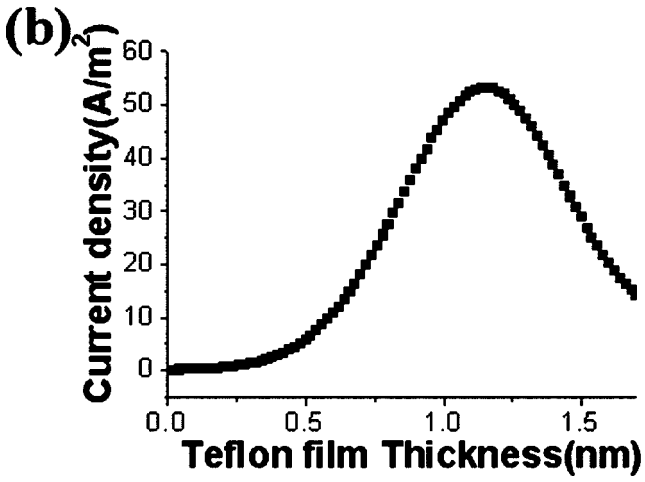

FIG. 8. (a) Numerical results on thickness dependence of the *I-V* characteristics through a flat teflon film of the hole-only device. (b) The calculated current of the hole-only device vs different thickness of the flat teflon film (under electric field of 0.2×10^7 V/cm).

Figure 8(a) shows the calculated *I-V* characteristics of the device with perfectly flat teflon film by Eq. (4), and Fig. 8(b) shows the current density under the electric field of 0.2×10^7 V/cm. It was found that the current density of the device with a perfectly flat teflon film was increased and reached a maximum at the thickness of 1.1 nm. These results agreed well with the experimental ones in Fig. 3.

Secondly, we numerically investigated the tunneling current through a rough teflon film in a hole-only device for comparison of the experiments in Fig. 5. By the morphology of teflon film with different thicknesses described in Fig. 4, the schematic diagram of the morphology of teflon films with

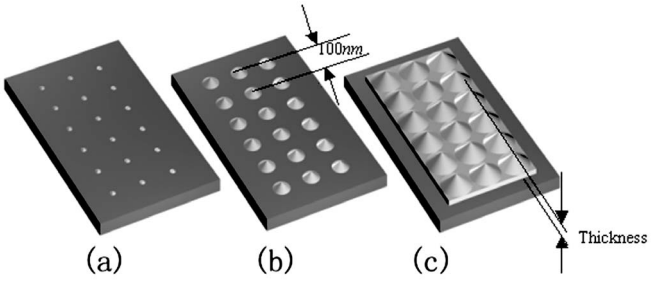

FIG. 9. (a), (b), and (c) show the morphology of a rough teflon film on ITO substrate with different thicknesses used in calculations. Cone-shaped islands were used as the teflon islands on ITO film and the ratio of height to bottom diameter of cone is 1:10. The space between two islands in the array is 100 nm.

different thicknesses used in our calculation was shown in Fig. 9. For simplicity, cone-shaped islands were used as the teflon islands on ITO film and the ratio of height to bottom diameter of cone is 1:10. The array of cone-shaped teflon islands on ITO film was used to describe the discontinuous teflon film, shown in Figs. 9(a) and 9(b). The smallest space between two islands in the array is 100 nm. And Fig. 9(c) shows the morphology of the continuous teflon film used in the calculation. In Fig. 9, the thickness of the rough teflon film was defined as the distance from the top of the cone-shaped island to the ITO substrate.

Based on the above definition of rough teflon film, $U(x,y,z)$ and $T(y,z,p_x)$ on the surface S of the hole device can be calculated, and we also can calculate the tunneling current density $J(y,z)$ through an area element ds at the position (y,z) on the surface S. The average current density through the surface S of the device can be obtained by integrating $J(y,z)$ over the surface S. Figure 10(a) shows the calculated I-V characteristics of the devices with different thicknesses of the rough teflon film by Eq. (1), and Fig. 10(b) shows the calculated current density of devices under the constant electric field of 0.2×10^7 V/cm. These numerical results agreed well with experimental ones; for instance, in Figs. 5(a) and 10(a), the current density of devices linearly increases with teflon film thickness when the thickness of the rough teflon film is less than 8 nm. In Fig. 10(b), the current density of devices with different thicknesses of teflon film reached maximum twice, which was also similar to the experimental results in Fig. 5(b).

The numerical results in Fig. 10 reveal the physical process of holes tunneling through teflon film, as shown in Fig. 11. Because the tunneling current density $J(y,z)$ through the position (y,z) on the surface of teflon film was calculated to be maximum for the 1.1 nm thick teflon film in Fig. 8, the tunneling current through a rough teflon film in the device was mainly contributed by holes tunneling through the area of teflon film with the thickness of about 1.1 nm. When teflon film is discontinuous and teflon islands were small, the tunneling current was mainly through the top of teflon islands into Alq. When the islands grew, the fringe of the teflon islands became the main area where holes tunneled through. And when the teflon islands coalesced, the valleys among the islands of teflon film were the area where holes

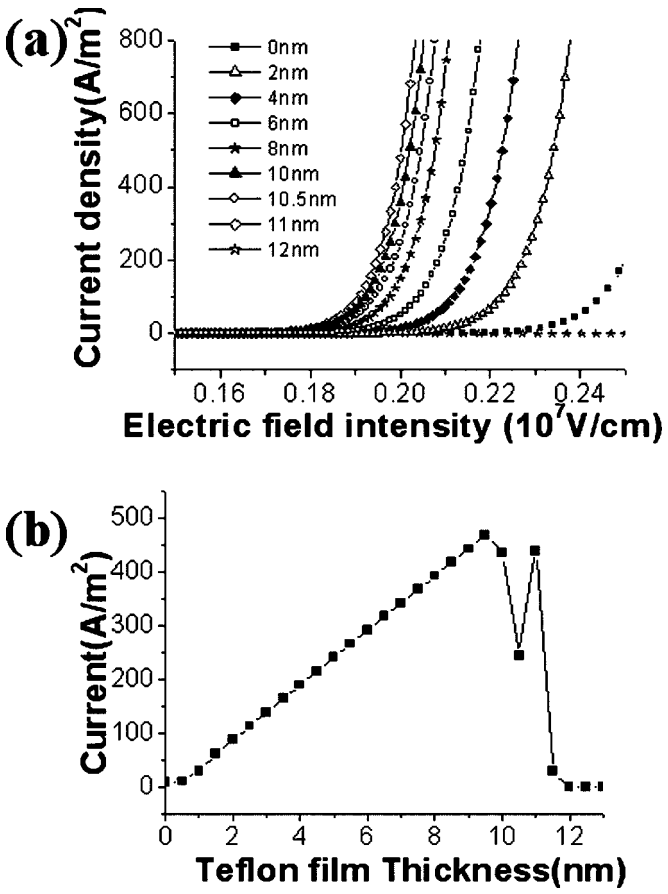

FIG. 10. (a) Numerical results on thickness dependence of the I-V characteristics through a rough teflon film of the hole-only device. (b) The calculated current of the hole-only device vs different thicknesses of the rough teflon film (under electric field of 0.2×10^7 V/cm).

tunneled through. In Fig. 10(b), the two peaks of current density of devices resulted from the maximum of tunneling current through islands and valleys of the rough teflon film with different thicknesses respectively, and the pit in the curve of current density for the thickness of 10.5 nm came from the attenuation of tunneling current through the fringes

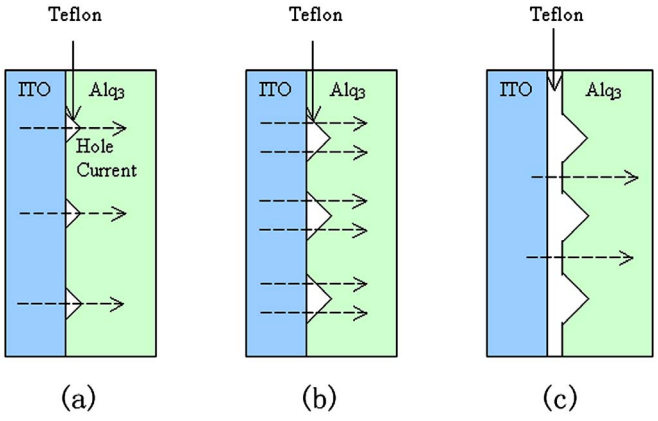

FIG. 11. (Color online) Schematic diagram of holes tunneling through the rough teflon film with different thicknesses in devices.

of islands and the increasing of tunneling current through the valleys when the rough teflon film grew.

This picture of carriers tunneling through a rough teflon film also could be partly applied to the tunneling effect of other insulator films such as LiF (Ref. 5) and NaSt,[17] which do not have a perfectly flat surface. From our numerical results and understanding of the tunneling effect through the teflon film, the discrepancy between theoretical and experimental optimal thickness of LiF film in previous work[5] could also be attributed the roughness of LiF film.[6] More importantly, our theoretical study revealed that carrier injections by the tunneling effect through thin insulator films are localized, that is, carriers are injected not through the entire interface but the localized area of the insulating film, causing the formation of carrier channels in the bulk of the organic semiconductor. The formation of carrier channels is expected to affect the charge recombination efficiency and performance of organic light-emitting diodes.

V. CONCLUSION

In conclusion, we investigated hole tunneling injection through the structure of an electrode (ITO)/insulator (teflon)/organic semiconductor (Alq) both experimentally and theoretically. In the experiment, we found that the hole current was enhanced by the tunneling effect of teflon film, and affected by the morphology of teflon film. We developed a theoretical tunneling model based on WKB approximation. By considering the morphology of teflon film in the calculation, the experimental results can be explained well, which provided further understanding of tunneling injection through the thin insulator film. In the presented physical picture of tunneling injection of carriers through an insulator film, the rugged surface of the insulator film will induce the localized injection of carriers and lead to current channels in the organic semiconductor, which is expected to have a serious impact on the characteristics and performance of organic electronic devices.

ACKNOWLEDGMENTS

This work was supported by the National Natural Science Foundation of China under Grants No. 90101029 and No. 50173014, and the National Key Basic Research and Development Program of China under Grant No. 2002CB613405.

APPENDIX: THE DETAILED THEORETICAL MODEL AND CALCULATIONS

Based on the WKB approximation of one-dimensional Schrödinger equation, the transmission coefficient of the energy barrier was shown as follows:[19]

$$T \approx \exp\left(-2\int_{x1}^{x2} \eta dx\right), \tag{A1}$$

$$\eta = \left\{\frac{2m}{\hbar^2}[U(r)-E]\right\}^{1/2}, \tag{A2}$$

where E is the energy of the particle, $U(r)$ is the potential energy, and m is the particle effective mass. We just considered the particle transmission through the energy barrier along the x direction, then Eq. (A2) can be expressed as

$$\eta = \left\{\frac{2m}{\hbar^2}\left[U(r)-\left(\frac{p_x^2}{2m}\right)\right]\right\}^{1/2}. \tag{A3}$$

The flux of particles incident on the barrier with x component of momentum between p_x and p_x+dp_x is

$$Flux = 2(p_x/m)g(E,p_x)f(E)dp_x dE, \tag{A4}$$

where $g(E,p_x)$ is the density of state and $f(E)$ is the Fermi-Dirac function. Based on the free-electron model, the density of state $g(E,p_x)$ could be calculated to be $2\pi m/(2\pi\hbar)^3$.[19] The maximum number of particles per unit time which could cross the barrier along the x direction in the energy and momentum ranges considered is

$$(Flux)T(p_x) = 2(p_x/m)T(p_x)g(E,p_x)f(E)dp_x dE. \tag{A5}$$

In this paper, we considered the tunneling transmission from ITO to Alq through the teflon layer, and neglected the interfacial state, the space charge limitation in Alq, and reverse transmission from Alq to ITO, then transmission current through the area element ds between p_x and p_x+dp_x, E and dE is

$$J(E,p_x)\vec{e}_x\cdot\vec{n}dp_x dE ds = 2(p_x/m)T(y,z,p_x)g(E,p_x)f(E)\vec{e}_x\cdot\vec{n}dp_x dE ds \tag{A6}$$

where $\vec{n}$ is a unit vector normal to the area element ds of the surface S, and $\vec{e}_x$ is the unit vector of x direction.

The total current through the surface S and over all possible values of p_x and E can be obtained by integrating Eq. (A6),

$$I_{tot} = \int\int\int J(E,p_x)\vec{e}_x\cdot\vec{n}dp_x dE ds. \tag{A7}$$

And the average current density through the surface S can be expressed as

$$\bar{J} = I_{tot}/S = \int\int\int J(E,p_x)\vec{e}_x\cdot\vec{n}dp_x dE ds \Big/ S \tag{A8}$$

Substituting Eq. (A6) into (A8), integrating and simplifying Eq. (A8) yields

$$\bar{J} = \left(\frac{K_b T}{2\pi^2\hbar^3}\right)\left\{\int\int \vec{e}_x\cdot\vec{n}ds dp_x p_x T(y,z,p_x) \times \ln\left[1+\exp\left(\frac{E_f - p_x^2/2m}{K_b T}\right)\right]\right\} \Big/ S. \tag{A9}$$

If the teflon film was uniform and the surface S between teflon and Alq was perfectly flat, the transmission coefficient $T(y,z,p_x)=T(p_x)$, and tunneling current density $J(y,z)=J$ at the position (y,z) on the surface S were independent on the y and z component in space. Thus the average transmitting current density through the surface S is

$$\bar{J} = J = \left(\frac{K_b T}{2\pi^2 \hbar^3}\right) \int dp_x p_x T(p_x) \ln\left[1 + \exp\left(\frac{E_f - p_x^2/2m}{K_b T}\right)\right]. \tag{A10}$$

If the surface S is not perfectly flat and teflon film is rough, then $T(y,z,p_x)$ varies on the surface S. The average transmitting current density through the entire surface S can be calculated by

$$\bar{J} = \left(\frac{K_b T}{2\pi^2 \hbar^3}\right) \left\{ \int\int\int \cos(\theta) dy dz dp_x p_x T(y,z,p_x) \times \ln\left[1 + \exp\left(\frac{E_f - p_x^2/2m}{K_b T}\right)\right] \right\} \Big/ S. \tag{A11}$$

where θ is the angle between $\vec{n}$ and $\vec{e}_x$.

*Corresponding author. Email address: chldwang@tsinghua.edu.cn
†Corresponding author. Email address: qiuy@tsinghua.edu.cn

[1] Y. E. Kim, H. Park, and J. J. Kim, Appl. Phys. Lett. **69**, 599 (1996).
[2] L. S. Hung, C. W. Tang, and M. G. Mason, Appl. Phys. Lett. **70**, 152 (1997).
[3] X. J. Wang, J. M. Zhao, Y. C. Zhou, X. Z. Wang, S. T. Zhangm, Y. Q. Zhan, Z. Xu, H. J. Ding, G. Y. Zhong, H. Z. Shi, Z. H. Xiong, Y. Liu, Z. J. Wang, E. G. Obbard, W. Huang, and X. Y. Hou, Appl. Phys. Lett. **95**, 3828 (2004).
[4] B. J. Chen, X. W. Sun, K. S. Wong, and X. Hu, Opt. Express **13**, 26 (2005).
[5] J. M. Zhao, S. T. Zhang, X. J. Wang, Y. Q. Zhan, X. Z. Wang, G. Y. Zhong, Z. J. Wang, X. M. Ding, W. Huang, and X. Y. Hou, Appl. Phys. Lett. **84**, 2913 (2004).
[6] F. Zhu, B. Low, K. Zhang, and S. Chua, Appl. Phys. Lett. **79**, 1205 (2001).
[7] P. Piromreun, H. Oh, Y. Shen, G. G. Malliaras, J. C. Scott, and P. J. Brock, Appl. Phys. Lett. **77**, 2403 (2000).
[8] H. Tang, F. Li, and J. Shinar, Appl. Phys. Lett. **71**, 2560 (1997).
[9] F. Li, H. Tang, and J. Shinar, Appl. Phys. Lett. **70**, 1233 (1997).
[10] S. J. Kang, D. S. Park, S. Y. Kim, C. N. Whang, K. Jeong, and S. Im, Appl. Phys. Lett. **81**, 2581 (2002).
[11] Y. Q. Zhan, Z. H. Xiong, H. Z. Shi, S. T. Zhang, Z. Xu, G. Y. Zhong, J. He, J. M. Zhao, Z. J. Wang, E. Obbard, H. J. Ding, X. J. Wang, X. M. Ding, W. Huang, and X. Y. Hou, Appl. Phys. Lett. **83**, 1656 (2003).
[12] H. Jiang, Y. Zhou, B. S. Ooi, Y. Chen, T. Wee, Y. L. Lam, J. Huang, and S. Liu, Thin Solid Films **363**, 25 (2000).
[13] Yudi Gao, Liduo Wang, Deqiang Zhang, Lian Duan, Guifang Dong, and Yong Qiu, Appl. Phys. Lett. **82**, 155 (2003).
[14] L. S. Hung, R. Q. Zhang, P. He, and G. Mason, J. Phys. D **35**, 103 (2002).
[15] I. D. Parker, J. Appl. Phys. **75**, 1656 (1994).
[16] S. T. Zhang, X. M. Ding, J. M. Zhao, H. Z. Shi, J. He, Z. H. Xiong, H. J. Ding, E. G. Obbard, Y. Q. Zhan, W. Huang, and X. Y. Hou, Appl. Phys. Lett. **84**, 425 (2004).
[17] J. M. Zhao, Y. Q. Zhan, S. T. Zhang, X. J. Wang, Y. C. Zhou, Y. Wu, Z. J. Wang, X. M. Ding, and X. Y. Hou, Appl. Phys. Lett. **84**, 5377 (2004).
[18] T. C. Nason, J. A. Moore, and T. M. Lu, Appl. Phys. Lett. **60**, 1866 (1992).
[19] A. T. Fromhold, Jr., *Quantum Mechanics for Applied Physics and Engineering* (Dover, New York, 1991).